

A Long-Stroke Nanopositioning Control System of the Coplanar Stage

Hung-Yu Wang, Kuang-Chao Fan, Jyun-Kuan Ye, and Chung-Hao Lin

Abstract—With the continuing trend toward device miniaturization in many engineering and scientific fields, the need to accomplish highly precise measurements at the micro- or nanoscale has emerged as a critical concern. This paper presents a high-precision motion control system for the nanopositioning of a coplanar X – Y stage driven by two commercial ultrasonic motors. The motor drive provides three main driving modes, namely ac, Gate, and dc, for millimeter, micrometer, and nanometer displacements, respectively. The displacement of each axis stage is sensed using a linear diffraction grating interferometer (LDGI) with a nanometer resolution. To compensate for the effects of the variable friction force during stage motion, the gains of the proportional–integral–derivative controller used to regulate the stage motion are tuned adaptively by a back propagation neural network (BPNN) based on the feedback signals provided by the LDGI. Furthermore, to obtain a high-accuracy positional motion, the error compensation strategy is implemented to eliminate the systematic errors of the stage with error budget. The error budget is obtained by positioning error calibration using a laser interferometer, which optical axis is detected by a quadrant photodetector (QPD) to ensure no cosine error. The positioning accuracy of the proposed system is evaluated by performing a series of contouring experiments. The results demonstrate that the system achieves a nanometer level of accuracy and resolution and is, therefore, a suitable solution for micro-coordinate measuring machine, microlithography, and micromachining applications.

Index Terms—Back propagation neural network (BPNN), contouring control, coplanar stage, error compensation, linear diffraction grating interferometer (LDGI).

I. INTRODUCTION

LONG-STROKE and nanopositioning systems with nanometer-level resolution and accuracy are critically important for nanotechnology [1]. Although piezoelectric nanopositioning systems are designed to provide the greatest possible positioning accuracy, in practice, they exhibit a number of non-ideal characteristics. For the high-bandwidth application, lots of mechanical amplifications and control strategies have been performed in the last decade [2]–[4]. As of today, lots of nanotechnologies have been widely implemented by piezoelectric actuators, such as scanning probe microscope [5], nanotechnologies

Manuscript received June 9, 2012; revised October 24, 2012; accepted December 10, 2012. Date of publication January 14, 2013; date of current version January 17, 2014. Recommended by Technical Editor Y. Sun. This work was supported in part by the National Science Council of Taiwan under Grant NSC 98-2221-E-002-143.

The authors are with the Department of Mechanical Engineering, National Taiwan University, Taipei 10617, Taiwan (e-mail: d96522010@ntu.edu.tw; fan@ntu.edu.tw; r98522723@ntu.edu.tw; r99522711@ntu.edu.tw).

Color versions of one or more of the figures in this paper are available online at <http://ieeexplore.ieee.org>.

Digital Object Identifier 10.1109/TMECH.2012.2235455

TABLE I
COMMERCIAL NANOSCALES

Maker / Model	Scale pitch	Resolution	Accuracy
SONY / BL55 http://sonypt.com/spt_products.asp	1.6 μm	10 nm	$\pm 2.5 \mu\text{m}$
Heidenhain / LIP382 http://www.heidenhainencoders.co.uk/heidenhain-lip382-lip300_58	512 nm	31.25 pm	$\pm 0.5 \mu\text{m}$
OPTRA / NanoScale Model A http://www.optra.com/nanoscale.html	10 μm	5 nm	$\pm 200 \text{ nm}$
MicroE / Mercury II 6000 series http://www.microsys.com/m2/m2-6000.html	20 μm	1.2 nm	$\pm 1 \mu\text{m}$
Renishaw / TONiC http://www.renishaw.com/en/tonic-linear-encoders--10186	20 μm	1 nm	$\pm 1 \mu\text{m}$

[6], [7], optical alignment [8], [9], and coordinate measuring machines, etc. [10], [11].

In general, the long-stroke stage for nanopositioning is always regarded as expensive equipment as it normally requires a high-precision two-stage assembly for long-and-short motions. Commercial X – Y stages usually comprise two linear stages with one stacked on top of the other and provide displacements in the X - and Y -directions, respectively [12]–[15]. However, even though the two stages may individually possess a nanoscale positioning accuracy; it is extremely difficult to achieve good positioning performance due to assembly errors, component misalignment, control error, and so on. In practice, the performance of high-precision measurement and fabrication machines is constrained by the Abbé principle. In [16], the authors compensated for the effects of the Abbé offset error in coordinate measuring machine (CMM) systems by means of a new error correction strategy. By contrast, in this study, the Abbé offset error is eliminated completely by confining the X - and Y -motions of the stage to a single common plane.

In implementing a nanopositioning system, highly precise sensors are required to measure the displacement of the stage over an extended travel distance. Some commercial linear optical encoders are commonly adopted. Such devices, however, have a relatively large grating pitch, and thus the resolution is inevitably constrained [17]. Although with high interpolation factors the scale reading can be up to nanometer, but all are with accuracy in micron or submicron level only. Table I lists some commercial nanoscales that can be found from individual website. A laser interferometer provides a more precise solution for long-displacement measurement to nanometer resolution and accuracy. However, laser interferometer systems not only require a highly precise alignment and assembly process, but also need a sophisticated system to accomplish temperature control and vibration isolation [18]. In recent years, grating interferometry

has emerged as a means of solving the paradox between the measuring range and the resolution [19]. For example, in [20], the present group proposed a linear diffraction grating interferometer (LDGI) capable of sensing stage displacements with a resolution of 1 nm over a travel distance of 20 mm.

Ultrasonic motor, which utilizes sliding friction as the driving force [21], [22], can provide a mechanically straightforward approach for stage actuation. However, the positioning performance of such motors is highly sensitive to variations in the surface roughness of the driven stage. Accordingly, an effective control system is required to ensure a precise positioning of the stage, particularly when performing low-speed and long-stroke displacements. Conventional proportional–integral–derivative (PID) controllers are ineffective when the surface roughness varies so significantly that large variations in the stage velocity occur [23]. To overcome this problem, various self-tuning controllers have been proposed. For example, Tanaka *et al.* [24] demonstrated the precise positioning of an ultrasonic motor using a PID controller integrated with a neural network (NN). Zhao *et al.* [25] proposed a control scheme comprising a PID controller and a back propagation fuzzy NN. However, the proposed method was not verified experimentally. Seniyu *et al.* [26] developed an ultrasonic motor control system based on a back propagation neural network (BPNN). The results showed that the proposed system enabled a precise control of the ultrasonic motor. However, the experimental results were obtained using only a simulated load. Lin *et al.* [27] presented a recurrent fuzzy NN method for controlling the ultrasonic motor drivers of an X – Y stage. However, a rapid polling time was required to acquire the feedback signal needed to accomplish the synchronous nanopositioning of the two axes.

In a previous study [28], the present group developed an intelligent nanopositioning control system comprising a self-designed coplanar stage driven by commercial ultrasonic motors, two LDGI displacement sensors, and a fuzzy cerebella model articulation controller. However, the performance of the controller was adversely affected by the fluctuations induced in the LDGI feedback signal at the excitation frequency of the ultrasonic motors. Thus, while the short-stroke control of discrete steps with a micro- or nanoscale resolution was successfully achieved, an accurate long-stroke positioning control could not be obtained.

This study proposes an improved nanopositioning system in which the displacement of the coplanar stage is controlled by a BPNN-based self-tuning PID controller. Different from the previous configuration [29], in this study, the actuator and the displacement sensor are positioned at opposite ends of the stage, thereby improving the stability of the LDGI feedback signal. Furthermore, to construct a coplanar stage for long-stroke and nanopositioning the effort will be more difficult as all error sources have to be considered, such as the drive error, guide error, scale error, geometric error, environment error, control error, etc. The previous study [30] proposes the nanopositioning control for 1-D and this study implements error compensation strategy including “home accuracy,” “position accuracy,” and “backlash error” in both axes. The positioning performance of the proposed system is evaluated by means of a series of contour-

ing experiments. The results confirm that the system achieves a reliable positioning performance in all the three motion modes, namely ac, Gate, and dc.

From the aforementioned explanation, it is known that in the field of nanopositioning technology, many efforts are made on the paradox between resolution and travel range when working at a multiscaled range. In spite of some achievements, the studies on the integration of different driving modes into an all-in-one controller, signal processing for new sensors, friction disturbance, and closed-loop control for long-time position locking are still a challenging task. Moreover, the necessity of perfect optical alignment of the laser beam to the calibrated axis must be proven for nanometer accuracy. These are the novelty of the proposed methods in this report. This paper is organized as follows.

The description of a designed coplanar X – Y stage, which is based on the Abbé principle and sensed by LDGI.

The driving system, which consists of an ultrasonic motor and the driver.

The control algorithm, which utilizes BPNN to fine-tune PID parameters.

The error compensation scheme, which is established by error mapping to enhance the positioning accuracy.

Experimental verification with positioning control and contouring control.

II. STRUCTURE OF THE LONG-STROKE AND NANOPositionING COPLANAR STAGE

A. Design of a Coplanar X – Y Stage

As described previously, conventional X – Y stages generally comprise a stacked arrangement of two linear stages. However, the stacked arrangement results in a position-dependent cross-talk error between the two axes, and thus the positioning performance of the stage is seriously degraded. Moreover, the displacement of the lower stage is subject to a large Abbé error due to the large vertical Abbé offset.

To resolve these limitations, this study proposes a novel coplanar Abbé-free X – Y stage. As shown in Fig. 1, the moving table slides over a common base plane, which is precisely ground to a flatness error of less than 1 μm and is isolated from the drive and sensing blocks. In order to ensure a smooth motion of the table, concave grooves are formed on the base plane using a scraping process and are filled with liquid lubricant to minimize the sliding friction force between the moving table and the base plane. Fig. 2 presents a photograph of the assembled coplanar stage. The table is surrounded by four linear slides, each of them is connected by a linear stage. Two orthogonal stages are driven by respective ultrasonic motors and drivers. Each axis displacement of the table is detected by a corresponding LDGI sensor, whose output is used as a feedback signal in achieving a precise positioning of the stage.

In assembling the stage, the LDGI sensors were carefully aligned to ensure that the grating axis was parallel to the moving axis and the LDGI laser beam was normal to the grating surface. In addition, the straightness of the two moving slides and the flatness of the moving table were calibrated using a

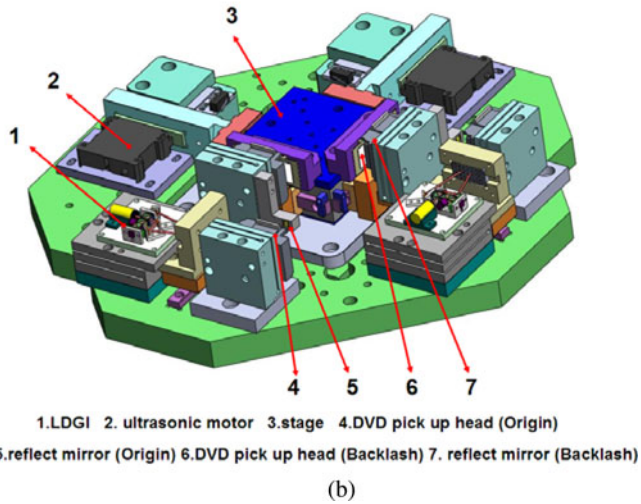
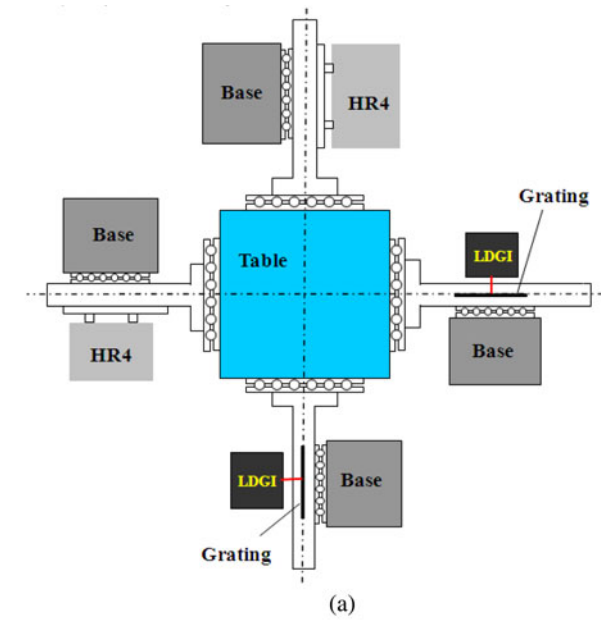


Fig. 1. (a) General layout of the coplanar Abbé-free X - Y stage and (b) 3-D rendered model of the coplanar X - Y stage.

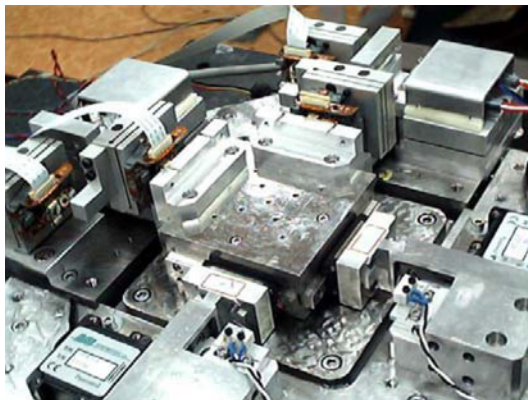


Fig. 2. Photograph of assembled coplanar X - Y stage.

TABLE II
HR4 SPECIFICATIONS

HR4 USM Specification	
Maximum Permissible Velocity	250 mm/s
Dynamic Stall Force	15 to 18 N
Static Holding Force	14 N (reference value)
Input Wave Form and Frequency	39.6kHz, sin wave
Maximum Voltage	270 Vrms

TABLE III
AB2 DRIVER SPECIFICATIONS

AB2 Driver Specification	
Power Input	24V \pm 5%
Max. Motor Output	280 Vrms
Input Voltage range	\pm 10V
Input Low Pass Filter	2.7kHz
Mode type	AC/ Gate/DC
DC Mode Output Range	\pm 300nm

laser interferometer prior to attaching the linear guides to the base plate. The inspection results showed that both the straightness and flatness errors were less than 50 nm. Having attached the linear guides to the base plate, their orientation was carefully adjusted using a flexure mechanism.

B. Ultrasonic Motor

As shown in Fig. 2, the X and Y axes are each driven by an actuator system comprising an ultrasonic motor (Nanomotion Co., model HR4) and a driver amplifier (model AB2). The technical specifications of the ultrasonic motor and driver amplifier are shown in Tables II and III, respectively.

To displace the slide, the driver amplifier applies an excitation voltage across four piezo ceramic elements mounted on the ultrasonic motor. Given a precise control of the sequence in which the voltage is applied, an elliptical motion of the tips attached to each element is induced. The ultrasonic motors are positioned such that the tips are in contact with the slide. Thus, the elliptical tip motion displaces the slide by means of a friction force. Detailed operation principle has been reported in [30].

C. Principle of Sensors

To achieve the nanopositioning motion, highly precise sensors are required to measure the displacement and compensate the systematic error of the coplanar stage. This study proposes LDGI as a displacement sensor, whose output is used as a feedback signal. To eliminate the systematic errors of the stage with error budget, DVD pick up heads [29] are used to set up the machine origin and compensate the backlash error of the slide in each axis. Furthermore, this study proposes a perfect alignment method, which utilizes a quadrant photodetector (QPD) to assist the alignment of the beam of a laser interferometer with respect to the motion axis during the calibration of positional

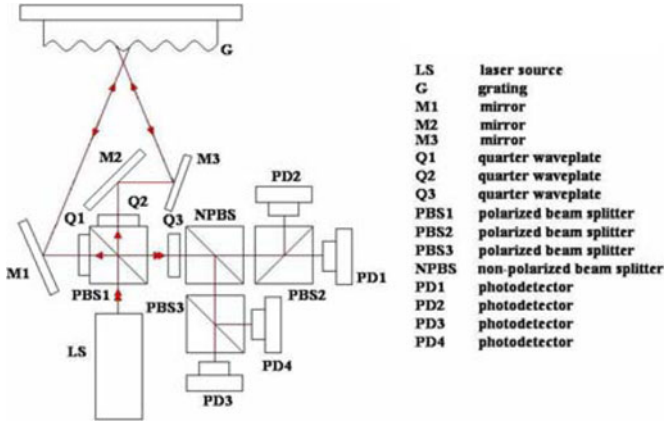


Fig. 3. Optical structure of the LDGI displacement sensor.

errors. Detailed information will be introduced in the following sections.

1) *LDGI*: Fig. 3 shows the optical system of the LDGI system. The laser diode (LS) emits a linearly polarized beam, which is split by a polarization beam splitter (PBS1) into two beams with equal intensity. Each beam emits to the grating (G) at the first-order diffraction angle so that each diffracted beam will return back along the same path, being a Littrow configuration. The optical system design adopts polarization technique so that the returned beams will not enter into the laser diode but travel to the right-handed side for encoding the interference signals by one NPBS, two PBS, and four photodetectors. Detailed operation principle has been reported in [20].

The intensities of the output signals generated by the four photodetectors can be expressed as follows:

$$\begin{aligned} I_{PD1} &= 2A^2[1 + \cos(\Delta\omega t)] \\ I_{PD2} &= 2A^2[1 - \cos(\Delta\omega t)] \\ I_{PD3} &= 2A^2[1 + \sin(\Delta\omega t)] \\ I_{PD4} &= 2A^2[1 - \sin(\Delta\omega t)]. \end{aligned} \quad (1)$$

The displacement Δx of the grating scale (pitch d) is related to the phase difference of the first-order diffraction of the grating surface by means of the following equation:

$$\Delta\omega = 4\pi \frac{\Delta x}{d}. \quad (2)$$

When the grating moves a half-pitch, the beat frequency signal has a phase variation of one period (360°). With a holographic grating of 1200 lines/mm, there is a wave cycle of the orthogonal signals at every 416 nm of the grating movement.

2) *Quadrant Photodetector*: QPD is composed of four photo cells of equal quadrant size. As shown in Fig. 4, when the spot projects at different position, each of photo cells will output voltage corresponding to the spot projecting area. An analog electronic circuit can process output signals and convert them to the corresponding X and Y positions of the beam, expressed by

$$X = \frac{(V_A + V_D) - (V_C + V_B)}{V_A + V_B + V_C + V_D} \quad (3)$$

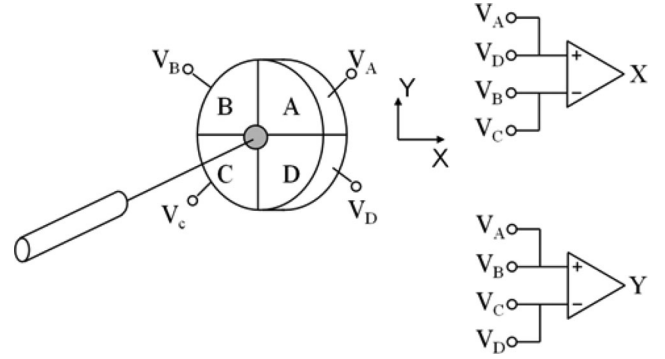


Fig. 4. Principle of the QPD.

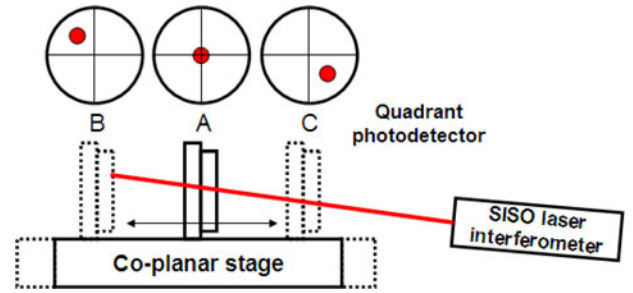


Fig. 5. Schematic diagram of misalignment between the laser beam and the moving axis.

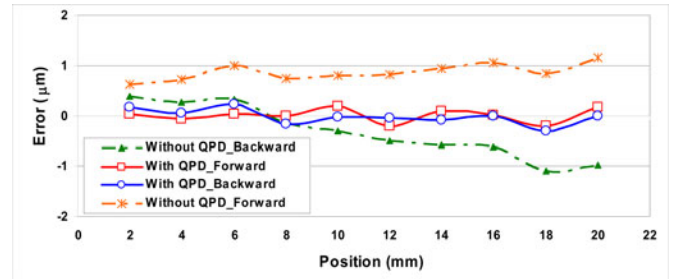


Fig. 6. Optical axis calibration with QPD.

$$Y = \frac{(V_A + V_B) - (V_C + V_D)}{V_A + V_B + V_C + V_D}. \quad (4)$$

A current positioning error calibration method for any precision linear stage adopts a laser interferometer as a reference to compare with the actual positional readings of the stage. As shown in Fig. 5, any misalignment of the laser beam to the moving axis will cause cosine errors, especially in the ultra-high precision long-stroke stage. A current alignment method based on the light intensity of the reflected beam is too human dependent that can never assure perfect alignment. In this study, a QPD is employed to assist the optical alignment so that the laser beam can be adjusted to allow projecting onto the detector the same position both at near end and far end of travel. As shown in Fig. 6, the position errors in forward and backward motions have good performance having adjusted by the QPD. This innovative QPD-assisted laser

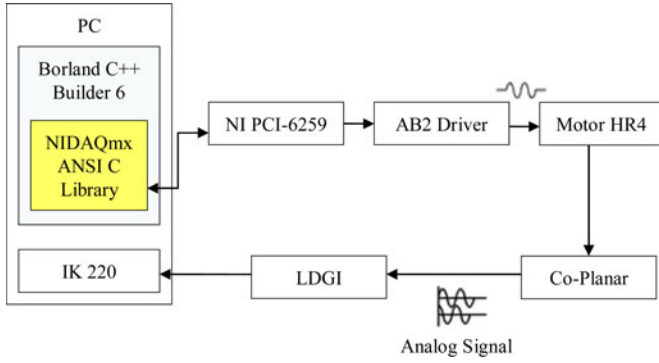


Fig. 7. Block diagram of control loop for the coplanar X - Y stage.

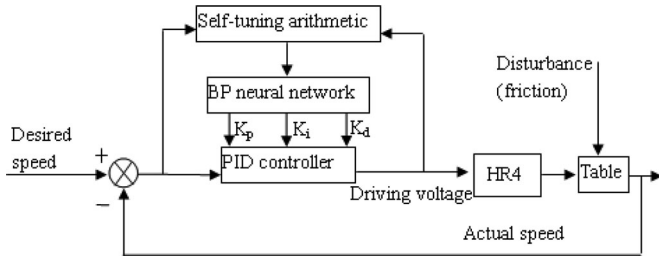


Fig. 8. Block diagram of the self-tuning PID controller.

calibration method is called the “perfect alignment method” in this study.

III. CONTROL MOTION SYSTEM

The motion control system for the coplanar stage comprises an actuation system (two ultrasonic motors and associated driver amplifiers), a displacement sensing system (two LDGI sensors), and a self-tuning PID controller. Fig. 7 presents a block diagram of the control system. The controller is programmed in Borland C++ Builder and the control signals are interfaced to the driver via a NI PCI 6259 DAQ (Data Acquisition) cards (National Instrument Co.). The waveforms output from LDGI are decoded by an interpolation card (IK220 of Heidenhain Co.) to nanometer resolution.

A. Self-Tuning PID Control Algorithm

PID controllers have been used in many practical control applications. In the coplanar stage developed in this study, the base plane is not perfectly smooth. The friction force acting on the base plate of the moving table varies during the motion, causing unstable velocity. Consequently, the gains of the PID controller must be adjusted in real-time in order to achieve a smooth motion. As shown in Fig. 8, the gains are tuned adaptively by means of a BPNN [31], [32], in accordance with the difference between the desired speed of the driven slide and the actual speed. In constructing the BPNN, the total input to each neuron j is defined as follows:

$$\text{net}_j^n = \sum W_{ij} Y_i^{n-1} - \theta_j \quad (5)$$

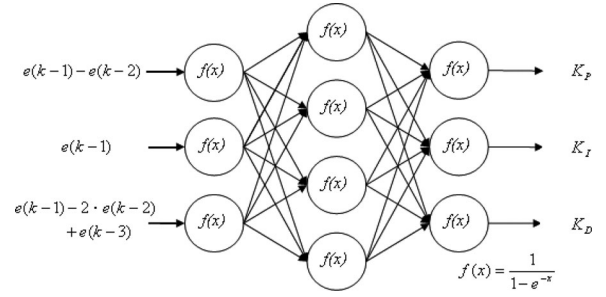


Fig. 9. Structure of BPNN used to tune gains of the PID controller.

where θ_j is a predefined threshold value. Meanwhile, the output of each neuron j is obtained as

$$Y_j^n = f(\text{net}_j^n), \quad f(x) = \frac{1}{1 + e^{-x}}. \quad (6)$$

The BPNN-based PID controller is then formulated as

$$u(k) = K_P e(k) + K_I \sum_{j=0}^k e(j) + K_D [e(k) - e(k-1)] \quad (7)$$

where, K_P , K_I , and K_D are proportional, integral, and derivative gains, respectively. $u(k)$ is the plant input, and $e(k)$ is the error between a desired value $r(k)$ and the actual output $y(k)$, such that

$$e(k) = r(k) - y(k). \quad (8)$$

In the proposed control system, the BPNN comprises three layers. As shown in Fig. 9, each of the input and output layers comprises three nodes. The nodes in the input layer receive $e(k-1)-e(k-2)$, $e(k-1)$, and $e(k-1)-2e(k-2)+e(k-3)$ as inputs, while those in the output layer provide K_P , K_I , and K_D as outputs. Finally, the hidden layer is configured with four nodes. In implementing the BPNN, the cost (error) function is defined as

$$E = \frac{1}{2} \sum_j (r(k) - y(k))^2 = \frac{1}{2} e^2(k). \quad (9)$$

Equation (9) expresses the difference between the desired output $r(k)$ and the actual output $y(k)$. Thus, the objective of the BPNN is to determine the PID gains which minimize the cost function.

In this study, the BPNN was used to learn two parameters, namely the driving voltage and the slide speed variation. During the training process, the connection weights were adjusted in accordance with (9) by means of the steepest descent method [33].

B. Characteristics of Driving Modes

For a long stroke and nanopositioning of the coplanar stage, three motion modes are employed by AB2 driver. The AB2 driver provides three main driving modes, namely an ac mode for millimeter displacement, a Gate mode for micrometer displacement, and a dc mode for nanometer displacement. The details of three modes' switching have been reported in [30].

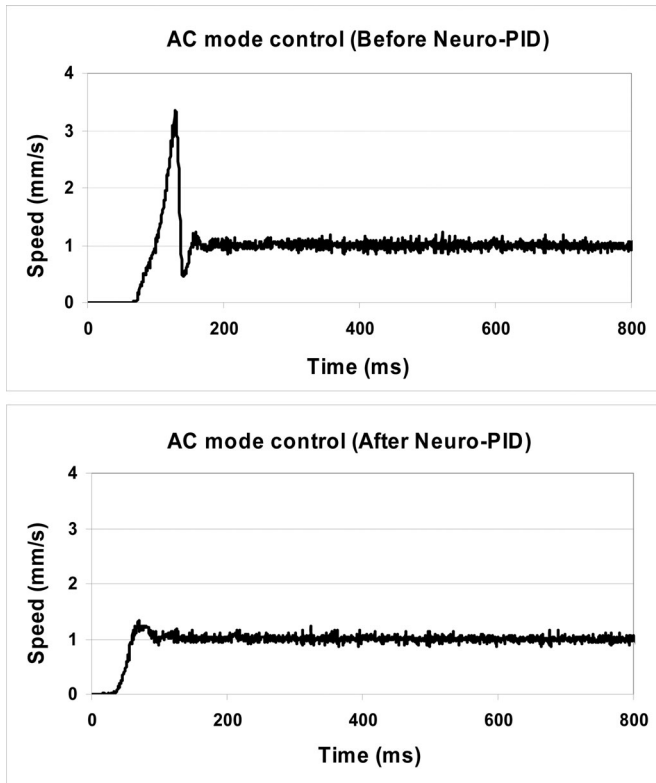


Fig. 10. AC-mode control by the static (upper) and the self-tuning (lower) PID controller.

The similar strategy is used in this study, i.e., once the moving table is close to the target point within $5\ \mu\text{m}$, the ac mode will switch to the Gate mode, which will switch to the dc mode if the target position is within $100\ \text{nm}$. The characteristics of each mode and its corresponding control strategy will be performed in the following sequence.

Since the base plane of the coplanar X - Y stage is not perfectly smooth, the slide velocity varies during displacement. The variation in the driving speed is particularly apparent in the initial phase of the displacement process due to the static friction effect [34], [35]. The developed X - Y stage has low damping, and thus an overshoot in the slide velocity occurs when the stage is first actuated if an adequate control is not applied. In the ac mode, the input variable is the commanded voltage, which is proportional to the speed of motion, and the output variable is the displacement, which will determine the instantaneous speed and feedback to the BPNN loop. Fig. 10 shows the speed control performance obtained in the ac mode when using a conventional PID controller (upper) and the BPNN-based PID controller (lower). It is evident that the BPNN-based controller successfully eliminates the overshoot phenomenon in the initial displacement period and suppresses the variation in the slide velocity over the entire displacement process.

In the Gate mode, a stepwise movement of the stage is achieved by applying a series of periodic ON/OFF*** pulses to the ultrasonic motors. The step size is determined by the magnitude of the applied voltage, while the displacement speed is determined by the pulse width. As shown its step response in

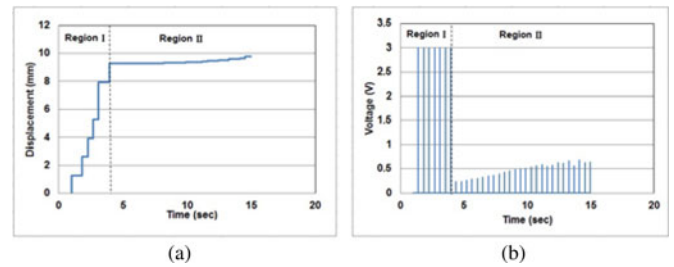


Fig. 11. Gate-mode step response control. (a) Displacement versus time. (b) Voltage versus time.

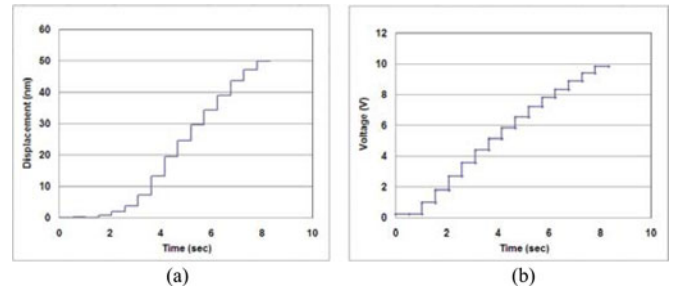


Fig. 12. DC-mode step response control. (a) Displacement versus time. (b) Voltage versus time.

Fig. 11, the voltage signal used to achieve a displacement of $10\ \mu\text{m}$ in the Gate mode comprises two regions, namely Region I, corresponding to large steps, and Region II, corresponding to very small steps, performed under the control of the BPNN PID controller. Once reached a distance of less than $100\ \text{nm}$ from the final target position the control system switches to the dc mode.

During dc motion, the stage velocity is precisely controlled using the BPNN-PID controller with a high polling cycle time in order to achieve a precise nanopositioning performance and lock at the target position. Fig. 12 shows the step response of dc mode motion which is conducted at different voltage levels with the same voltage range of $0.5\ \text{V}$. The displacement which is not proportional to the voltage due to friction is varying at every position; a close-loop control scheme is thus necessary in the dc mode.

C. Error Compensation Scheme on the Coplanar Stage

The contouring error [36], [37] is defined by normal distance between the actual trajectory and the commanded path, and can be evaluated as a function of tracking errors to the reference path. Although a lot of high-resolution drivers and precision transmission mechanisms have been proposed, however, they are all difficult to achieve nanoposition accurately due to the systematic errors in the component assembly. In order to meet such a requirement, it is necessary to develop the error compensation scheme. This paper presents the error compensation strategy including “home accuracy,” “position accuracy,” and “backlash error” in both axes.

To achieve the nanometer accuracy of the coplanar stage, compensation for the positioning errors is necessary. Based on this demand, it is necessary to establish the error budget for compensation. Before creating that, both the X and Y axes

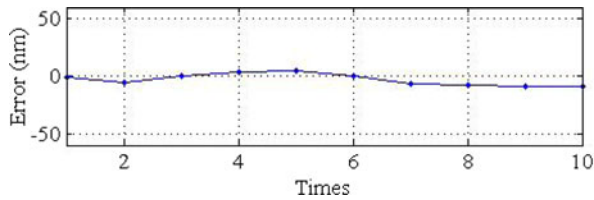


Fig. 13. Home positioning error.

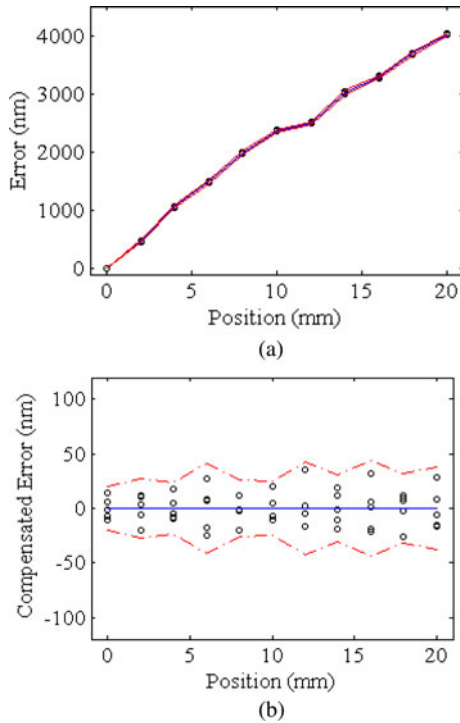


Fig. 14. Accuracy tests by the laser interferometer: (a) before error compensation and (b) after error compensation.

need a reference point (or called the machine origin) in the coordinate system. As shown in Fig. 1, part 4 of the DVD pick-up head is fixed to the baseplate. It uses its focus error signal (FES) to detect the gap with a reflective mirror mounted on the stage. The reference point of the moving axis is thus set when the FES is zero. From this point, the laser interferometer (MI 5000, SIOS) is used to calibrate the positioning error of the moving axis. This is also called the absolute positioning error calibration. The homing error is about 5 nm with a standard deviation around 5 nm, as shown in Fig. 13.

For positioning error compensation, the absolute positions relative to home are stored in the error budget for feed-forward error compensation. Each target position has been attained five times for the travel range up to 20 mm. As shown in Fig. 14, the positioning error can be controlled to ± 20 nm with standard deviation 12 nm after implementing error compensation.

Another error that would influence the positioning error is the backlash of the linear slide between the moving table and the LDGI stage. This is the inherent clearance variation between the slide and the guide under different loads. As shown in Fig. 15, a DVD sensor (part 3) is employed to detect this backlash when the table is changed the motion direction.

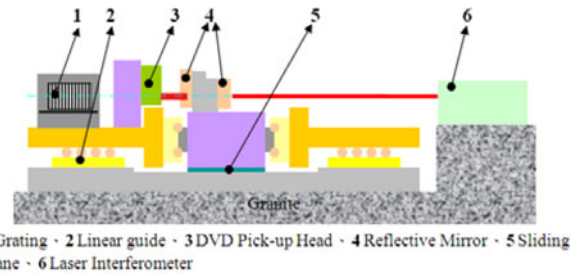


Fig. 15. Schematic diagram of backlash compensation.

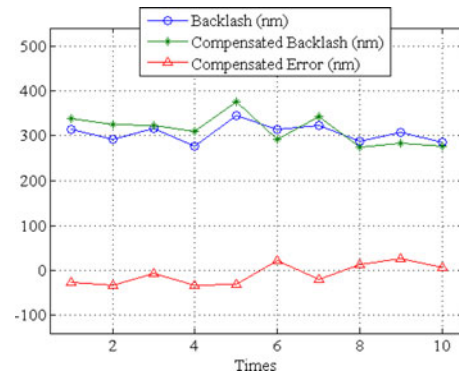


Fig. 16. Backlash error compensation.

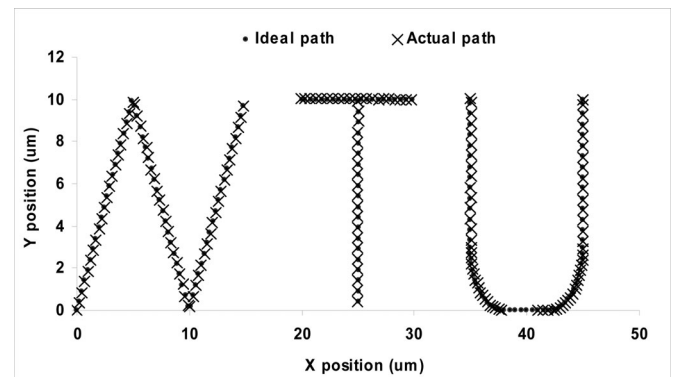


Fig. 17. Evaluation of contouring control.

The amount of backlash can be accurately measured by the FES signals to nanometer level. As shown in Fig. 16, the original backlash of about 300–400 nm has been reduced to about 20 nm with standard deviation 12 nm after error compensation.

IV. EXPERIMENTAL TESTS

A. Contouring Control of the Coplanar Stage

The effectiveness of the BPNN-PID controller was demonstrated by performing a series of contouring experiments. The results presented in Fig. 17 confirm the ability of the coplanar stage to trace a path comprising both straight and curved sections. The contouring errors can be controlled to less than 19 nm. Figs. 18 and 19 show that the stage is capable of tracing paths comprising straight segments and right-angle turns with contouring errors less than 10 nm.

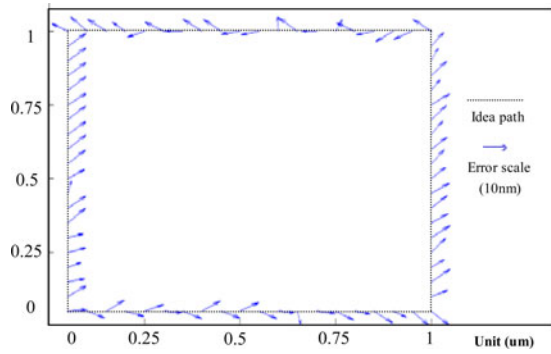


Fig. 18. Evaluation of square contouring control.

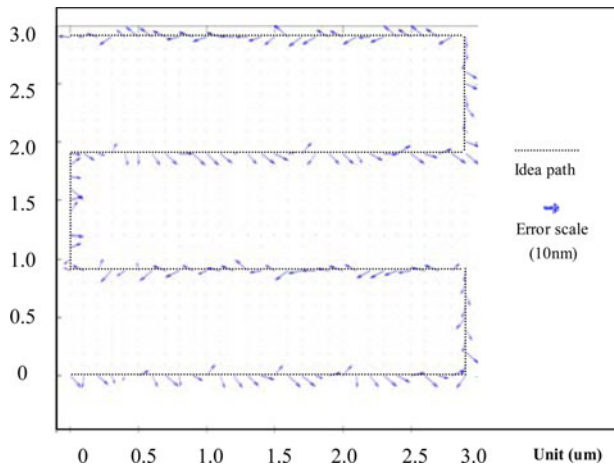


Fig. 19. Evaluation of the grating contouring control.

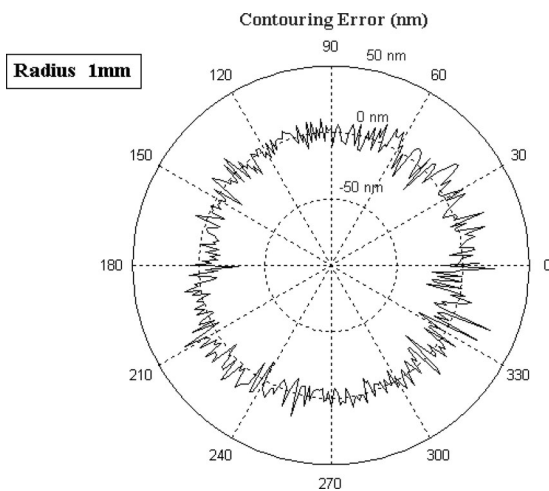


Fig. 20. Evaluation of the circular contouring control.

B. Circular Test of the Coplanar X–Y Stage

The ability of the BPNN to simultaneously adjust the gains of X and Y control loops was demonstrated by tracing a circular path. Fig. 20 presents the results obtained for a circular path with a radius of 1 mm. The radial deviations of the actual path from the specified path are found to be within 25 nm.

V. CONCLUSION

This paper has presented a high-precision motion control system for an Abbé-free coplanar X – Y stage comprising two ultrasonic motors and associated drivers, two LDGI displacement sensors, and a BPNN-based self-tuning PID controller. The control system supports three different driving modes, namely an ac mode for millimeter displacement, a Gate mode for micrometer displacement, and a dc mode for nanometer displacement. It makes the multiscale displacement driven by a single actuator possible. The employed LDGI is featured with long-stroke and nanometer resolution/accuracy. The velocity can be controlled in smooth motion after applying the BPNN-PID scheme to eliminate the friction-induced disturbance at the start-up by ac mode and at the target approaching by dc mode. The proposed perfect alignment method ensures the calibration result of positional accuracy without cosine error. Besides, the error compensation strategy is established by error mapping to enhance the positioning accuracy. The experimental results have shown that the coplanar stage is capable of performing both straight and curved (or circular) motions with a nanoscale level of positioning accuracy. These results demonstrate that stage has significant potential for applications such as micro-CMM, micromachining, micro-lithography, and so forth.

REFERENCES

- [1] S. Devasia, E. Eleftheriou, and S. O. R. Moheimani, "A survey of control issues in nanopositioning," *IEEE Trans. Control Syst. Technol.*, vol. 15, no. 5, pp. 802–823, Sep. 2007.
- [2] R. Yang, M. Jouaneh, and R. Schweizer, "Design and characterization of a low-profile micropositioning stage," *Precis. Eng.*, vol. 18, no. 1, pp. 20–29, Jan. 1996.
- [3] Y. Li and Q. Xu, "Design and robust repetitive control of a new parallel-kinematic XY piezostage for Micro/Nanomanipulation," *IEEE/ASME Trans. Mechatronics*, vol. 17, no. 6, pp. 1120–1132, Dec. 2012.
- [4] B. J. Kenton and K. K. Leang, "Design and control of a three-axis serial-kinematic high-bandwidth nanopositioner," *IEEE/ASME Trans. Mechatronics*, vol. 17, no. 2, pp. 356–369, Apr. 2012.
- [5] H. T. H. Chen, W. Ng, and R. L. Engelstad, "Finite element analysis of a scanning x-ray microscope micropositioning stage," *Rev. Sci. Instrum.*, vol. 63, no. 1, pp. 591–594, Jan. 1992.
- [6] P. Mckeown, "Nanotechnology-special article," in *Proc. Nano-metrology Precis. Eng.*, Hong Kong, 1998, pp. 5–55.
- [7] B. A. Awaddy, W.-C. Shih, and D.-M. Auslander, "Nanometer positioning of a linear motion stage under static loads," *IEEE/ASME Trans. Mechatronics*, vol. 3, no. 2, pp. 113–119, Jun. 1998.
- [8] H. Marth and B. Lula, "Development of a compact high-load PZT-ceramic long-travel linear actuator with picometer resolution for active optical alignment applications," *Proc. SPIE*, vol. 6273, pp. 62731k-1–62731k-5, 2006.
- [9] B. Tamadazte, N. Le Fort-Piat, and E. Marchand, "A direct visual servoing scheme for automatic nanopositioning," *IEEE/ASME Trans. Mechatronics*, vol. 17, no. 4, pp. 728–736, Aug. 2012.
- [10] K. C. Fan, Y. T. Fei, X. F. Yu, Y. J. Chen, W. L. Wang, F. Chen, and Y. S. Liu, "Development of a low-cost micro-CMM for 3D micro/nano measurements," *Meas. Sci. Technol.*, vol. 17, no. 3, pp. 524–532, Mar. 2006.
- [11] K. Takamasu, R. Furutani, and S. Ozono, "Development of nano-CMM (Coordinate Measuring Machine with Nanometer Resolution)," in *Proc. XIV IMEKO World Congr.*, 1997, vol. 8, pp. 34–39.
- [12] P. Yang, T. Takamura *et al.*, "Development of high-precision micro-coordinate measuring machine: Multi-probe measurement system for measuring yaw and straightness motion error of XY linear stage," *Precis. Eng.*, vol. 35, no. 3, pp. 424–430, Jul. 2011.
- [13] K. S. Low and M. T. Keck, "Advanced precision linear stage for industrial automation applications," *IEEE Trans. Instrum. Meas.*, vol. 52, no. 3, pp. 785–789, Jun. 2003.

- [14] S. Polit and J. Dong, "Development of a high-bandwidth XY nanopositioning stage for high-rate Micro-/Nanomanufacturing," *IEEE/ASME Trans. Mechatronics*, vol. 16, no. 4, pp. 724–733, Aug. 2011.
- [15] Y. Li and Q. Xu, "A novel piezoactuated XY stage with parallel, decoupled, and stacked flexure structure for micro-/nanopositioning," *IEEE Trans. Ind. Electron.*, vol. 58, no. 8, pp. 3601–3615, Aug. 2011.
- [16] J. B. Bryan and D. L. Carter, "Design of a new error-corrected co-ordinate measuring machine," in *Proc. Precis. Eng.*, 1979, vol. 1, no. 5, pp. 125–128.
- [17] X. H. Chen, Y. Zhao, and D. C. Li, "Review on optical nanometrology," *J. Opt. Tech.*, vol. 3, pp. 74–78, 1999.
- [18] J. Kramar, "Nanometre resolution metrology with the molecular measuring machine," *Meas. Sci. Technol.*, vol. 16, no. 11, pp. 2121–2128, Nov. 2005.
- [19] S. G. Rautian, "On the theory of interferometers with diffraction gratings," *Opt. Spectrosc.*, vol. 93, no. 6, pp. 934–940, Dec. 2002.
- [20] F. Cheng and K. C. Fan, "Linear diffraction grating interferometer with high alignment tolerance and high accuracy," *Appl. Opt.*, vol. 50, no. 22, pp. 4550–4556, Aug. 2011.
- [21] M. Yang, B. Hanson, M. C. Levesley, P. G. Walker, and K. Watterson, "Amplitude modulation drive to rectangular-plate linear ultrasonic motors with vibrators dimensions 8 mm /spl times/ 2.16 mm /spl times/ 1 mm," *IEEE Trans. Ultrason., Ferroelectr., Freq. Control*, vol. 53, no. 12, pp. 2435–2441, Dec. 2006.
- [22] J. Maas, T. Schutle, and N. Frohliche, "Model-based control for ultrasonic motors," *IEEE/ASME Trans. Mechatronics*, vol. 5, no. 2, pp. 165–180, Jun. 2000.
- [23] S. Cong and Y. Liang, "PID-like neural network nonlinear adaptive control for uncertain multivariable motion control system," *IEEE Trans. Ind. Electron.*, vol. 56, no. 10, pp. 3872–3879, Oct. 2009.
- [24] K. Tanaka, M. Oka, A. Uchibori, Y. Iwata, and H. Morioka, "Precise position control of an ultrasonic motor using the PID controller combined with NN," *Trans. Inst. Electr. Eng. Jpn. C*, vol. 146, no. 3, pp. 46–54, Feb. 2004.
- [25] X. Zhao, W. Chen, and S. Shi, "Ultrasonic motor's velocity control based on the BP fuzzy neural network with stored information," in *Proc. 1st Int. Symp. Syst. Control Aeronautics*, 2006, pp. 1140–1144.
- [26] T. Senjyu, H. Miyazato, S. Yokoda, and K. Uezato, "Speed control of ultrasonic motors using neural network," *IEEE Trans. Power Electron.*, vol. 13, no. 3, pp. 381–387, May 1998.
- [27] F. J. Lin, R. J. Wai, K. K. Shyu, and T. M. Liu, "Recurrent fuzzy neural network control for piezoelectric ceramic linear ultrasonic motor drive," *IEEE Trans. Ultrason., Ferroelectr., Freq. Control*, vol. 48, no. 4, pp. 900–913, Jul. 2001.
- [28] K. C. Fan and Z. F. Lai, "An intelligent nano-positioning control system driven by an ultrasonic motor," *Int. J. Precis. Eng. Manuf.*, vol. 9, no. 3, pp. 40–45, Apr. 2008.
- [29] K. C. Fan, C. L. Chu, and J. I. Mou, "Development of a low-cost auto-focusing probe for profile measurement," *Meas. Sci. Technol.*, vol. 12, no. 12, pp. 2137–2146, Dec. 2001.
- [30] F. Cheng, K. C. Fan, L. Miao, B. K. Li, and H. Y. Wang, "A BPNN-PID based long-stroke nanopositioning control scheme driven by ultrasonic motor," *Precis. Eng.*, vol. 36, no. 3, pp. 485–493, Jul. 2012.
- [31] S. Omatu and M. Yoshioka, "Self-tuning neuro-PID control and applications," in *Proc. IEEE Int. Conf. Systems, Man and Cybernetics*, Oct. 1997, vol. 3, pp. 1985–1989.
- [32] F. C. Chen, "Back-propagation neural networks for nonlinear self-tuning adaptive control," *IEEE Control Syst. Mag.*, vol. 10, no. 3, pp. 44–48, Apr. 1990.
- [33] R. Fletcher and M. J. D. Powell, "A rapidly convergent descent method for minimization," *Comput. J.*, vol. 6, no. 2, pp. 163–168, Jan. 1963.
- [34] A. Ferreira, "Optimized friction drive controller for a multi-DOF ultrasonic nanopositioner," *IEEE/ASME Trans. Mechatronics*, vol. 9, no. 3, pp. 481–490, Sep. 2004.
- [35] H. Shakir and W.-J. Kim, "Nanoscale path planning and motion control with maglev positioners," *IEEE/ASME Trans. Mechatronics*, vol. 11, no. 5, pp. 625–633, Oct. 2006.
- [36] G. C. Chiu and M. Tomizuka, "Contouring control of machine tool feed drive systems: a task coordinate frame approach," *IEEE Trans. Control Syst. Technol.*, vol. 9, no. 1, pp. 130–139, Jan. 2001.
- [37] B. Yao, C. Hu, and Q. Wang, "An orthogonal global task coordinate frame for contouring control of biaxial systems," *IEEE/ASME Trans. Mechatronics*, vol. 17, no. 4, pp. 622–634, Aug. 2012.



Hung-Yu Wang was born in Taiwan on September 22, 1981. He received the B.S. degree from National Taiwan University of Science and Technology, Taipei, Taiwan, in 2003, and the M.S. degree from National Taiwan University (NTU), Taipei, in 2005, where he is currently working toward the Ph.D. degree, all in mechanical engineering.

His current research interests include metrology system integration.



Kuang-Chao Fan was born in Taiwan on January 4, 1950. He received the B.Sc. degree from National Taiwan University (NTU), Taipei, Taiwan, in 1972, the M.Sc. degree from the State University of New York, Buffalo, in 1976, and the Ph.D. degree from the University of Manchester Institute of Science and Technology, Manchester, U.K., in 1984, all in mechanical engineering.

He has been a Professor of mechanical engineering at NTU since August 1989. He was the Chairman of the Institute of Industrial Engineering, NTU, the Chairman of the Chinese Institute of Automation Technology, the Director of the Tjing Ling Industrial Research Institute, and the Associate Dean of the Engineering College, NTU. Since 2001, he has been the Yangtze Professor at the Hefei University of Technology, Hefei, China. His current research interests include manufacturing metrology, precision machining, machine tool technology, micro/nanomeasurement, optical switches, and tactile sensors.

Dr. Fan was the Chairman of the Society of Manufacturing Engineers Taipei Chapter.



Jyun-Kuan Ye received the M.S. degree from National Taiwan University (NTU), Taipei, Taiwan, in 2011.

He is currently a Field Assist Engineer at National Instruments. His current research interests include programming design.



Chung-Hao Lin received the M.S. degree from National Taiwan University (NTU), Taipei, Taiwan, in 2012.

He is currently an exchange student at the University of Oregon. His current research interests include nanometrology.